Journal of Statistical Physics, Vol. 64, Nos. 5/6, 1991

A Prepared Pattern with Wavelength Selection in Directional Solidification

P. E. Cladis[1]

As crystal growth is a vital link in the long chain of processes leading to state-of-the-art technological devices, a great deal is known about patterns formed at the solid–liquid interface of a growing crystal. However, some basic questions are still unanswered concerning macroscopic features exhibited by a moving solid–liquid interface. Even for the first instability, the cellular instability, a unique steady-state wavelength λ does not emerge from theory. Furthermore, while wavelength selection is observed in many different materials, its origin is still to be discovered. By breaking continuous rotational symmetry of the flat solid–liquid interface about the pulling direction $\mathbf{v}$, we prepared a cellular pattern with a well-defined wavelength by front propagation into the unstable uniform state. The material is succinonitrile and the rectangular interface geometry is formed by loading it into a flat capillary. The capillaries are chosen to provide a sample thickness $y_0 = 100\,\mu\text{m} \sim \lambda$, and width $10y_0$ and $20y_0$. We use a high-resolution directional solidification apparatus and grow the crystal from grain-boundary-free seed crystals. Surprisingly, the shape of the groove next to the uniform state is initially well-described by nearly self-similar Gaussians. This suggests that the initial perturbation of the interface is localized to a region $\lambda/2$ around a groove. A pattern with a well-defined wavelength is established when the half-width of the Gaussians $\xi_0 \sim 16\,\mu\text{m}$ is small compared to $\lambda \sim 80\,\mu\text{m}$ so there is little overlap between a groove and its predecessor or successor. When overlap is significant, the pattern is time-dependent. These results suggest that wavelength selection in this prepared pattern is a consequence of front propagation of a localized perturbation.

KEY WORDS: Directional solidification; pattern formation in nonlinear, dissipative systems.

[1] AT & T Bell Laboratories, Murray Hill, New Jersey 07974.

0022-4715/91/0900-1103$06.50/0

1. INTRODUCTION

Directional solidification is a model pattern-forming system[1] of the types of structures that can arise in nonlinear, nonequilibrium, dissipative systems.[2] In recent years there has been a surge in activity toward developing a conceptual framework for predicting the dynamical behavior of such systems that range from steady coherent structures to fully developed turbulence.[3] Similar to the major advance in critical phenomena,[4] the ambitious reach for a new level in understanding of pattern formation in nonequilibrium systems includes the search for a global description of the phenomena, a classification of singularities, and an understanding of universality properties.[5]

The cellular pattern emerges as a universal macroscopic structure (pattern) with wavelengths ranging from $\sim 10^3$ to $\sim 10^{-3}$ cm, in several nonlinear, nonequilibrium (driven) systems. Here, we mention only a few cases. Figure 1 shows a cellular pattern observed on the beach in El Segundo, California.[6] Its wavelength λ is ~ 25 feet, well-defined, and the largest we know. Similar patterns are observed in Langmuir–Blodgett films ($\lambda \sim 10\ \mu$m),[7] in the wetting process,[8] in a temperature gradient at the moving interface of liquid–liquid phase transitions ($\lambda \sim 40$–$140\ \mu$m),[9] in Saffman–Taylor experiments,[10] and at a gas–liquid interface in the "printer instability" ($\lambda \sim$ a few mm).[11]

As crystal growth is a vital link in the long chain of processes leading to state-of-the-art technological devices, the most well-studied cell pattern (however, only recently in the context of unanswered questions of pattern formation)[1] occurs in the solidification process,[12] the system we consider here. When the material is not a single-component system, the rough solid (crystal)–liquid interface exhibits a cellular pattern above a critical growth speed or pulling speed v_{cb} with $\lambda \sim 100\ \mu$m.

In their review, Hohenberg and Cross distinguish between "prepared patterns" and "natural" patterns.[5] They point out that prepared patterns should more closely resemble the "ideal" patterns of theorists. From an experimentalist's point of view, if a pattern can be prepared, then, clearly, that indicates some degree of control over the experiment. One is then encouraged to try new experiments to test the understanding implied by the ability to prepare a pattern.

Although not unknown in nature (e.g., snowflakes), a common feature of prepared patterns in the laboratory is that the scale of correlations is much larger than in "natural" patterns. For example, by introducing a weak oscillatory flow around a growing crystal, Bouissou *et al.*[13],[2]

[2] In this thesis, Bouissou notes that the parabolic character of a cell tip results when one considers that $z \sim t$ (driven), whereas $x \sim t^{1/2}$ (diffusion); therefore, $z \sim x^2$.

prepared a dendrite with periodic and correlated side-branching. Without this forcing, the dendrite side-branching is not correlated, so that large-scale features of its self-organization are less evident.[14] Owing to the larger scale, a clearer distinction can be made between features of the pattern due to noise[15] (e.g., noise-sustained structures[16]; e.g., Fig. 1?) and deterministic physical processes driving pattern formation in nonequilibrium systems.

Here we describe how we prepared a pattern in directional solidification of succinonitrile. The first step in its preparation is to use a confined

Fig. 1. The cellular pattern observed on the beach at El Segundo, California. It is not understood how this pattern forms. The wavelength of the cells is about 25 feet. (From ref. 6.)

geometry with well-defined boundary conditions at the perimeter of the interface. We call such an interface a *bounded interface* to distinguish it from one that is infinitely extended. The second step is to simulate front propagation of the cellular pattern into the unstable planar state by breaking the continuous rotational symmetry of the flat interface about **v**.

Let ψ symbolize a groove, the object that we propagate across the interface, and call ε a measure of distance from threshold. $\varepsilon < 0$ means that the driving force for pattern formation is below threshold, so ψ cannot grow as $\partial\psi/\partial t < 0$, where t is time. At threshold, $\varepsilon = 0$ and the pattern is marginally stable, $\partial\psi/\partial t = 0$. When $\varepsilon > 0$, the driving force is sufficiently large to form the pattern ($\partial\psi/\partial t > 0$), thus, $\psi \neq 0$.

As the pattern propagates across the interface, it provides a visual summary of ψ from below threshold ($\psi = 0$, the planar state and $\varepsilon < 0$) to above threshold ($\psi \neq 0$ and $\varepsilon > 0$). The change in ψ at a fixed position on the interface x_n is, in principle, related to distance from threshold ε. Thus, we studied a groove shape, centered at x_n, from onset to above threshold as the front swept by x_n. Near onset ($\varepsilon \gtrsim 0$), ψ, was two-dimensional and surprisingly well-described by nearly self-similar Gaussians, suggesting a response to a local perturbation where curvature effects are nonnegligible.

2. DIRECTIONAL SOLIDIFICATION AT THE SOLID–LIQUID INTERFACE

In directional solidification, a transparent alloy is placed in a temperature gradient **G**. The crystal state is forced to grow by pulling the sample at a constant speed **v** parallel to **G**, toward a cold contact.[17] Above a critical pulling speed[18] v_{cb}, the interface develops a cellular structure (wavelength $\lambda \sim 100\ \mu m$) often with deep grooves (Fig. 2).

Succinonitrile is the material used in these studies because its solid–liquid interface is rough, and it is transparent and chemically stable. Jackson and Hunt[19],[3] were the first to study, by direct visual observation, transparent materials in a temperature gradient. From their studies, we gained insight into the physial processes responsible for patterns at the growing crystal–liquid interface of metals and semiconductors. For example, Jackson was the first to point out that the cellular pattern occurs only at a rough solid–liquid interface[20]: on a microscopic scale, the interface is not defined. On the other hand, a faceted interface, well-defined on a microscopic scale, does not exhibit cells at any length scale. These facts link the cellular structure in solidification to the old and deep question of

[3] The materials they studied include succinonitrile, salol, carbon tetrabromide, and its eutectics.

pattern formation: how does disorder at small scales self-organize into order at large scales?[1]

The instability onset for an infinitely extended solid–liquid interface was first analyzed by Mullins and Sekerka.[18] As material solidifies behind a planar interface, a concentration gradient develops on the liquid side. In the steady state and when there is no diffusion in the solid state (one-sided approximation), then, on the liquid side, impurity increase by crystal rejection is balanced by impurity diffusion away from the interface. The result is an exponential profile for impurity concentration c as a function of distance z from the interface in the comoving frame $z = z' - vt$, the frame of reference attached to the flat interface. In this frame, the liquid is at $z > 0$ and the solid at $z < 0$ and the frame moves parallel to v.

At a planar interface, the characteristic length l_D associated with the exponential decay of $c(z)$ is given by D/v, with D the impurity diffusion constant in the liquid. The faster the crystal grows (larger driving force, v) the steeper the concentration gradient (smaller $l_D = D/v$). At an l_D such that the concentration gradient at the interface is greater than the equilibrium liquidus slope at T_L, a small perturbation of solid away from the solidus temperature into the liquid is in contact with liquid at a lower tem-

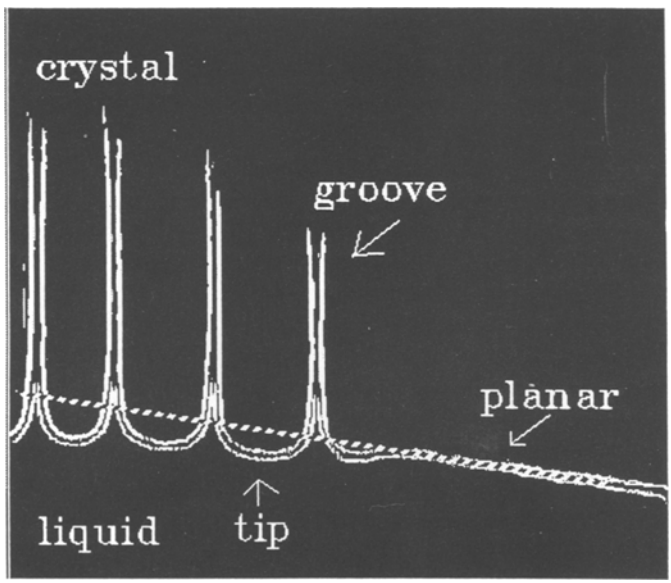

Fig. 2. The cell pattern consists of cell tips and grooves. The frame of reference is that z in a comoving frame is perpendicular and x parallel to the common tangent of the cell tips. y is out of the plane. The flat interface defines $z_I = 0$.

perature and concentration than the equilibrium T_L so it can grow despite the stabilizing effects of the thermal gradient (at long wavelengths) and surface effects (at short wavelengths).[21] This qualitative destabilizing mechanism of a planar interface is known as *constitutional supercooling* and has been quantified by Mullins and Sekerka for a sinusoidal perturbation of the interface.[18]

The experimental observation, in qualitative agreement with theory (see, e.g., ref. 22), is that the perturbation grows by moving to higher temperatures to form the tip feature of the pattern (Fig. 2). As the tip is at a higher temperature, the impurity concentration in the liquid at the tip (c_L^{tip}) decreases relative to that of the flat interface, c_L^0. Impurity loss at the tips is impurity gained by the grooves. Being richer in impurity than the tips, on both the solid and the liquid side of the interface, $c_L^{\text{groove}} > c_L^0 > c_L^{\text{tip}}$, the grooves extend away from the tips toward the cold contact (Fig. 2).

In a constant temperature gradient $|\mathbf{G}|$, temperature is mapped onto a spatial dimension z. In addition, the equilibrium phase diagram gives a linear relation between concentration of impurity at the interface and temperature. The interface position in $\mathbf{G}$, i.e., $z_I(x, y, t)$, corresponds to the melting temperature of $c_L(x, y, t)$ minus a correction due to the change in the melting temperature in the presence of curvature, κ.[4] Two more lengths emerge, the thermal length l_T and the chemical capillary length $\hat{d}$.

To see how these two lengths enter the problem, a small-amplitude sinusoidal perturbation in concentration,

$$\delta = \delta_0 \sin qx = \frac{c_L(x) - c_L^0}{c_\infty}$$

where c_∞ is the concentration in the liquid far from the interface, is applied to the flat interface.[18] The interface responds with $z_I = \zeta \sin qx$. Both δ_0 and ζ are small. Then,

$$-\delta(x) = \frac{z_I}{l_T} + \hat{d}\frac{d^2 z_I/dx^2}{[1 + (dz_I/dx)^2]^{3/2}} \approx \zeta\left(\frac{1}{l_T} - \hat{d}q^2\right)\sin qx \qquad (1)$$

In Eq. (1), $l_T = \Delta T/G$ with ΔT the width of the two-phase region associated with c_∞. From calorimetry measurements, we estimate $\Delta T \sim 3$ K. Thus, $l_T \sim 440\ \mu$m, while the chemical capillary length $\hat{d} \sim 200$ Å.[5] If

[4] In the Gibbs–Thompson effect, the sign of κ is chosen so that a "bump" of solid to higher temperatures melts, whereas a "bump" of liquid to lower temperature freezes.

[5] See, e.g., ref. 23 for a summary of the useful physical constants of succinonitrile. $\hat{d}_0$, the capillary length, is defined as the ratio of surface energy $\gamma = 9$ ergs/cm^2 to the latent heat/unit volume $T_m \Delta S_m = 4.6 \times 10^8$ ergs/cm^3. One has $\hat{d} = \hat{d}_0 T_m/\Delta T$.

$2\pi/q \gg 20\ \mu$m, curvature effects are small compared to $1/l_T$ and $z_I/l_T \sim -\delta(x)$.

Thus, for patterns where curvature effects are negligible, a 2D cell pattern is a visualization of impurity distribution at the interface. Studying macroscopic cell shapes and shape changes at the planar–cellular or cellular–side-branching bifurcations is a measure of the distribution/redistribution of impurities. The striking feature to emerge is that curvature supports an impurity deficit at the tips relative to the grooves. By increasing groove curvature, for a given $\delta(x)$, the groove extends further away from $z_I = 0$ than the tips that are comparatively weakly curved (Fig. 2). The cellular pattern in solidification, driven by curvature effects, is thus an important example of self-organization in a nonequilibrium system.

A broad band of wavelengths are unstable in the Mullins–Sekerka analysis, not just a single wavelength.[18] This raises the question, recently a subject of growing theoretical activity[24] in the context of pattern formation, of why the observed band is so small.

3. WAVELENGTH SELECTION

Roughly speaking, the interface overcomes the stabilizing effect of the thermal gradient (i.e., transforms or bifurcates to a cellular one) at a critical pulling speed v_{c1} when $l_D \sim l_T$.[1] In the weakly nonlinear regime, owing to continuous translatioal and rotational symmetry of the planar interface about **v**, periodic states can exist above threshold with a continuous band of wave numbers.[25,26] Given the available large band of wavelengths, why and how does the pattern choose one λ?

In a recent paper, Eshelman and Trivedi[27] dramatically demonstrated the magnitude of the discrepancy between theory and observation in directional solidification. They compared their observations on succinonitrile to the theoretical dependence of the critical speed on wave number for both marginally stable and fastest-growing wave number. On scales set by theory, all their data, spanning more than one decade in pulling speed v, lie on a nearly vertical line. In agreement, our observations are that while there is no long-range periodicity (only an average wavelength, $\langle\lambda\rangle$), when $v > v_{c2}$, the observed band is less than a factor of 2,[28] but with a strong dependence on sample thickness.

In practice, both pattern dynamics and wavelength selection are sensitive to sample thickness y_0. In theory, the interface, z_I is treated as infinite in one dimension (y) or both dimensions (x, y). In fact, when $y_0 \gg \langle\lambda\rangle \sim 40\ \mu$m, several rows of cells along y are formed resulting in a pattern that is difficult to study by image analysis. When $y_0 \ll \lambda$, the pattern is time dependent in wide samples ($-\infty < x < \infty$), whereas at long times,

$\lambda \sim 250\,\mu m \sim 5y_0$ in the bounded capillary geometry. Thus, boundary effects play a significant role in wavelength selection in experiments where the interface is never infinitely extended in either one or two dimensions. Indeed, they may be one of the strongest factors contributing to the large discrepancy between theories and observations. We will describe how boundary effects and front propagation can be used to prepare a pattern with a well-defined wavelength in samples where $y_0 \sim \lambda$.

For a supercritical bifurcation, Dee and Langer[29] first proposed front propagation as a dynamic wavelength selection mechanism: the wavelength is a unique function of the control parameter, $\varepsilon \sim v - v_{c1}$. The well-defined wavelength in the propagating pattern we prepare may be the first example of wavelength selection mediated by front propagation in directional solidification.[30] Although we succeeded in preparing a pattern, we cannot exclude the influence of other wavelength selection mechanisms, such as ramps (ε is a function of x)[31] and symmetry breaking.[32] A theoretical analysis is needed to answer questions on how these mechanisms compete or enhance each other in the selection process. For example, does front propagation in a ramp improve wavelength selection?

4. PREPARATION OF A PATTERN BY FRONT PROPAGATION

For our experiments, succinonitrile is vacuum-loaded into a flat glass capillary: width L, 1 or 2 mm; thickness, 100 μm; length, 50 mm. Measurements are made using a high-resolution directional solidification apparatus[28] and crystals grown from a defect-free seed crystal. We attribute the novel effects to be described to an impurity gradient parallel to the interface that develops in the capillary geometry when $v \sim v_{cb}$ because, initially, the interface is not perpendicular to $\mathbf{v} \parallel \mathbf{G}$ (Fig. 3).

We obtain a propagating mode by breaking the continuous rotational symmetry of the extended flat interface around $\mathbf{v}$ (and $\mathbf{G} \parallel \mathbf{v}$). However, the pattern that propagates one groove at a time into the planar state is asymmetric relative to $\mathbf{v}$ because of boundary effects.

In our apparatus, the maximum pulling distance, effected by a stepping motor (smallest step size 0.1 μm) is 25 mm. A frequency generator controls step rate to one part in 10^6. In these experiments, $G = 7.5$ K/mm and the separation between hot and cold contacts is 4 mm. A high-speed imaging system records the x–z plane through an automated video system attached to an optical microscope observing the interface along its smallest dimension, the y axis.

Grain-boundary-free seed crystals are obtained by repeatedly freezing then melting the sample in $\mathbf{G}$.[33] In addition, interface position measurements during melting give a value for the "dynamical" partition

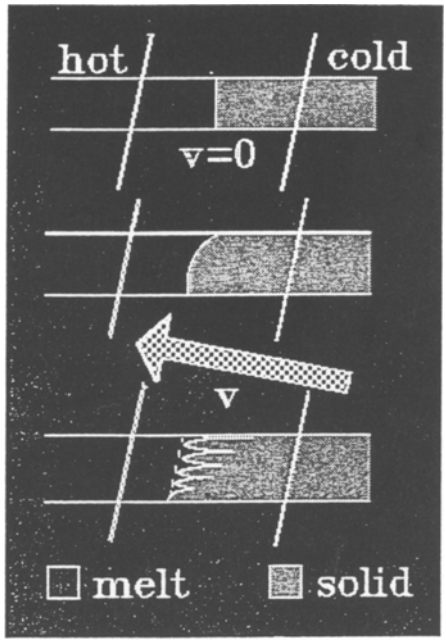

Fig. 3. Schematic of an $[x, z]$ plane of the experimental geometry to prepare patterns viewed along y, the thinnest dimension of the capillary, 100 μm. The edges of the hot and cold contacts are the slanted parallel lines. Both **G** and **v** are perpendicular to the edges of the hot and cold contacts that are 4 mm apart. The capillary (width 1 or 2 mm) is made up of the pairs of horizontal parallel lines at a small angle to **G** (in the experiment ~ 1.5–$3°$). Top: The sample is at rest and the interface is observed perpendicular to the capillary side walls. Middle: When $v \sim v_{cb}$, the planar interface develops a long-wavelength perturbation of amplitude A. Bottom: The cellular pattern propagates from the less pure end of the interface, i.e., the end closer to the cold contact. The dotted line tangent to the cell tips is perpendicular to $\mathbf{G} \parallel \mathbf{v}$. While cell tips are perpendicular to **v**, grooves are parallel to the side walls: the pattern is asymmetric.

coefficient k of 0.6[33] assuming a liquid impurity diffusion constant of 1.0×10^{-5} cm^2/sec.[6] We recall that for $k > 0.45$, the planar–cellular bifurcation is predicted to be supercritical.[35] Our method to determine v_{cb} is to measure the pulling distance d_u for the onset of the cellular pattern at different speeds,[36],[7] then plot $1/d_u$ vs. pulling speed v and extrapolate to zero to obtain a "bulk" critical pulling speed $v_{cb} = 1.12$ μm/sec.

[6] We do not know the impurity present in our samples; however, Chopra *et al.*[34] measure $D = 1.27 \times 10^{-5}$ cm^2/sec for succinonitrile/acetone and $D = 0.88 \times 10^{-5}$ cm^2/sec for succinonitrile/argon.

[7] The speed v is constant, so d_u is the product of v and the time for the cellular pattern to appear when $v > v_{cb}$. As $v \to v_{cb}$, $d_u \to \infty$. And when $v < v_{cb}$, d_u is undefined: the planar interface is stable. This method is useful if the interface becomes unstable everywhere at the same time, which it does when $v \gtrsim 3v_{cb}$.

When solidification begins with $v \sim v_{cb}$, the amplitude A (defined in Fig. 4) of a long-wavelength perturbation from the planar state increases from zero, peaks at A_{max}, then decreases when grooves begin to form (Fig. 4). A_{max} decreases linearly with v, is independent of sample width, and is zero when $v = v_{c2} = 2.9$ μm/sec (inset, Fig. 4). The amplitude A only grows while the interface is smooth, i.e., no grooves, $d < d_u$.

Our interpretation is the following. At rest, to minimize surface energy, the solid–liquid interface $z_I(x, 0)$ of succinonitrile in a capillary is perpendicular to the side walls and not to **G** even when the capillary is at a small angle (1.5–3°) to **G** (Fig. 3).[33] When solidification begins with **v** parallel to **G**, and while the interface is smooth ($d < d_u$), an impurity flux develops parallel to it because **v** has a component along the interface driving impurity away from $x = +L/2$ toward $x = -L/2$. When the interface is perpendicular to **v**, the sign of its component parallel to the interface changes, yet A continues to grow when $v < v_{c2}$. In a sense, we have made half of a large cell with its tip at $x = +L/2$ and its groove at $x = -L/2$.

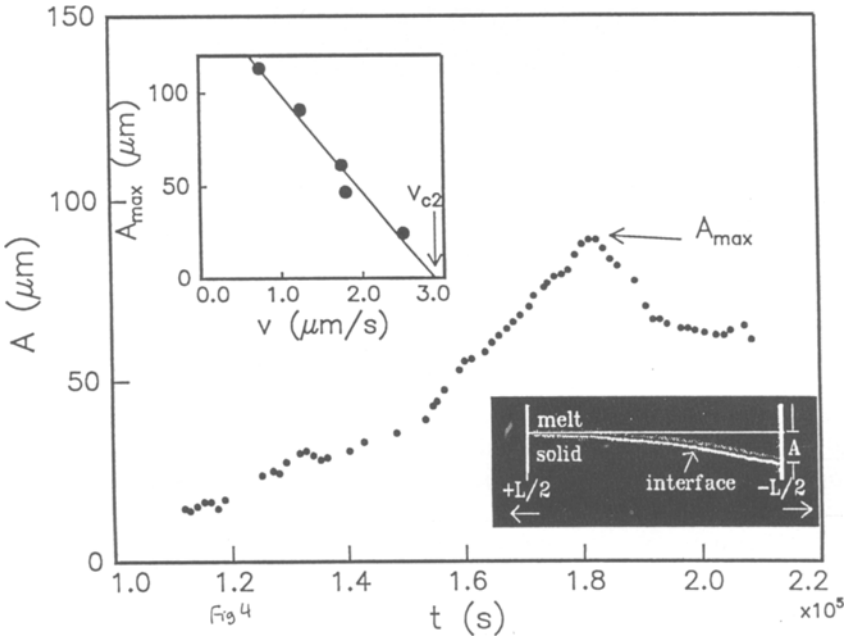

Fig. 4. Inset: Digitally enhanced image of the interface undergoing the initial long-wavelength distortion. The vertical white lines are shadows from the capillary side walls and the horizontal white line is the rest shape of the interface. The main figure shows the growth of the amplitude A vs. time t. At A_{max}, cells start to form at $-L/2$. Pulling speed $v = 1.25$ μm/sec. Smaller graph: A_{max} vs. v.

The interface is unstable first at $x = -L/2$ (Fig. 4). When d_u is large, $A_{\max}$ is large. When $v \gtrsim 3v_{cb}$, the planar–cellular transition occurs simultaneously everywhere on the interface, the effect is not observed, and the pattern is time-dependent.

When $v > v_{c1}$, grooves of liquid "propagate"[8] from the colder end of z_I to the warmer end (Fig. 5) at speed v_f. They stop at x_∞, where $x_\infty < L/2$ when $v \lesssim 2v_{c1}$, or, $x_\infty = L/2$ when $v \gtrsim 2v_{c1}$. The grooves remain parallel to the long axis of the capillary so their positions x_n are fixed. However, the common tangent of the cell tips is perpendicular to **v**, making the cell pattern asymmetric (Fig. 3). When $v = 1$ μm/sec, the time between successive groove formation (Fig. 5) is approximately $\tau \equiv D/v^2$, whereas at 2.5 μm/sec

[8] We use "propagate" for the groove pattern in the sense of van Saarloos,[37] i.e., the envelope of the groove pattern moves continuously across the interface, while a single groove keeps its place on the interface.

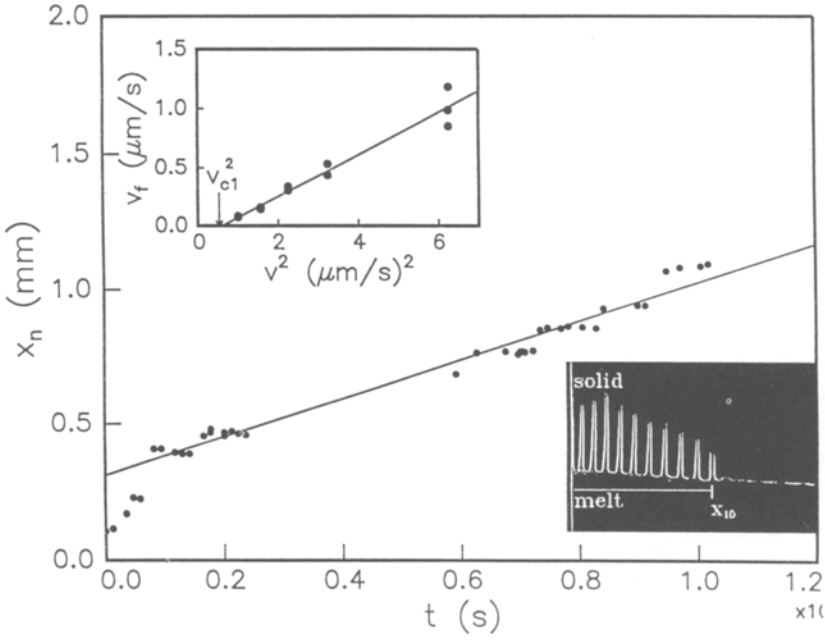

Fig. 5. Inset: Digitally enhanced image of cell pattern when x_∞ is at groove 11. Determination of the front speed v_f: position of the groove that leads the propagating pattern (x_n) as a function of time. $v = 1$ μm/sec. The front speed is different near the capillary edges. The gap in the data is where the magnification was increased to study the groove evolution in more detail (e.g., Fig. 6). Smaller graph: Front speed v_f vs. v^2. The slope is $\sim 2\lambda/D \pm 20\%$, i.e., $v_f \approx (2\lambda/D)(v^2 - v_{c1}^2)$.

it is closer to $\tau/2$. The smaller graph in Fig. 5 shows v_f as a function of v^2. The slope of the best line is $2\lambda/D \pm 20\%$, i.e., $v_f \approx (2\lambda/D)(v^2 - v_{c1}^2)$, giving $v_{c1} = 0.8$ μm/sec. When $0 < v < v_{c1}$, grooves do not occur.

The time between groove appearance is proportional to $\frac{1}{2}D/(v^2 - v_{c1}^2)$. In that time, the front travels a distance λ. As usual, a threshold increases the time as $v \to v_{c1}$. As noted above, when $v \gg v_{c1}$, the time between successive groove formation is half a diffusion time, whereas it is one diffusion time when $v = 1$ μm/sec $\sim 1.2 v_{c1}$.

When $v_{c1} < v < v_{c2}$, power spectra[33] of the groove patterns have a sharp peak at a $\lambda = 2\pi/q_0$ that varies from 81 ± 3 μm at $v = 1$ μm/sec to 70 ± 2 μm at $v \approx v_{c2}$. In contrast, the spectra for time-dependent patterns when $v > v_{c2}$ are too broad to determine λ.[33]

5. GROOVE SHAPE (ψ) SELECTION

While shape changes with pulling speed in the tip region have been studied in great detail with image analysis for stationary patterns[38] and traveling patterns,[39] very little is known about groove shapes. However, Weeks and van Saarloos[40] have studied the shape of deep grooves theoretically. In this limit a power-law behavior is expected (Scheil–Hunt law). Thus, the study of 2D grooves is a useful supplement to studies of the tip region that may shed some light on the wavelength selection problem in solidification. We will describe how a 2D groove grows[30] continuously from zero amplitude. Surprisingly, we found it was well-described by Gaussians.

The grooves we studied were the lead grooves of a cellular pattern that was propagating into the unstable planar state ($\psi = 0$). When the propagating pattern is observed at x_n, say, the control parameter ε is mapped onto time t. Before the front passes x_n, $\varepsilon < 0$ and $\psi = 0$. When the front arrives at x_n, the groove amplitude ψ is marginally stable ($\varepsilon = 0$). As the front passes, $|\psi|_{\max} \equiv f_1$ grows as ε increases. We observed $|\psi|_{\max}$ grow continuously from zero (at onset, $\varepsilon = 0$) to above threshold ($\varepsilon > 0$), where ψ became three-dimensional: $\psi(x, t) \to \psi(x, y, t)$.

Since grooves form sequentially in the propagating pattern and their center $|\psi|_{\max}$ is fixed, we analyzed the shape $[\psi: z_l(x, t)]$ of the lead groove in the pattern, i.e., the groove adjacent to the planar state. When $v_{c1} < v < v_{c2}$ and as a function of time, its shape is described by nearly self-similar Gaussians in x. Figure 6a shows the evolution of a lead groove z_l when $v = 1$ μm/sec $\sim v_{c1}$.

For convenience, we choose a frame of reference where $z_l - z_0 \geqslant 0$ is measured relative to the minimum of the pattern at z_0 (Fig. 6a). We digitized and fitted z_l to inflating Gaussians, $z_l = z_0 + f_1(t)(1 - f)$, where

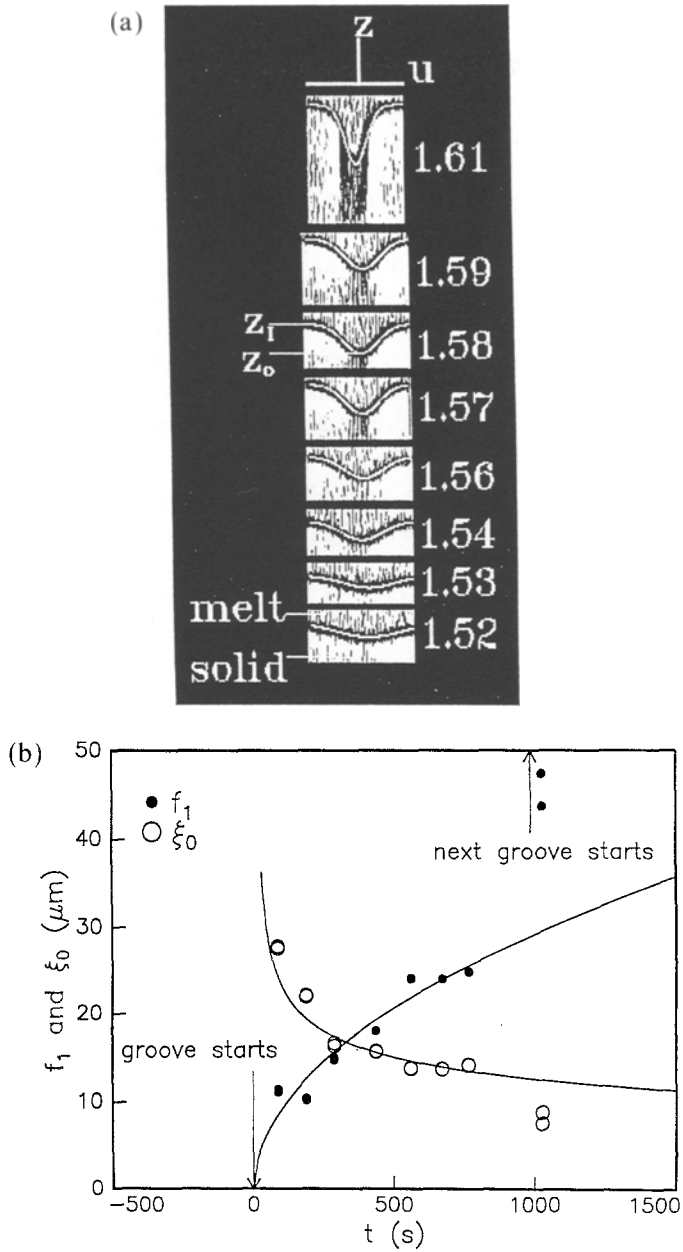

Fig. 6. (a) Images of lead groove formation when $A \neq 0$. The pulling distance d in mm is shown on the figure. $v = 1$ μm/sec and $d = d_0 + vt$. Here $z_l(u, t)$ is the interface between the solid and its melt. The groove amplitude is zero at $d_0 = 1.51$ mm. When the groove becomes three-dimensional between $d = 1.59$ and 1.61 mm, a new groove replaces it as pattern leader. The fits to Gaussians are the overlaid white lines. The vertical bar defining the z axis is 38 μm and the horizontal one defining the u axis is 79 μm. (b) Time dependence of the amplitude f_1 (●) and width ξ_0 (○) from the fits in part (a). The solid line for ξ_0 is a fit to $1/t^{1/4}$ and for f_1 to $t^{1/2}$, so $f_1 \sim 1/\xi_0^2$. The jumps in ξ_0 and f_1 correlate with the start of the growth of the next groove.

$f = \exp(-u^2/2\xi_0^2)$, $u = x - x_n$ and x_n is the groove center. The fit parameters f_1 and ξ_0 depend on time, while x_n and z_0 do not. The fitting error is $\sim 5\%$. When $t > \tau$, a new groove leads the pattern (next groove starts) correlating with jumps in both ξ_0 and f_1 (Fig. 6b) as well as the onset of 3D effects (Fig. 6a) in the retiring groove. This suggests that a stationary pattern of Gaussian grooves (no 3D effects) may be stabilized in a thinner sample (see, e.g., ref. 41).

Initially, ξ_0 decreases as $1/(d-d_0)^{1/4}$ and f_1 increases as $(d-d_0)^{1/2}$ (Fig. 6b). Here $d = d_0 + vt$ and d_0 is the pulling distance where a groove starts to grow. The fitted d_0 values agree with the observed values to $\pm 1\%$. Here $f_1\xi_0^2$ is a constant that should emerge from a theory of this process.

We note the following.

1. Taking all the measured points, $\langle \xi_0 \rangle = 16.2\,\mu$m, so that λ is approximately given by $5\langle \xi_0 \rangle$. While the overlap between the Gaussian of a groove and its predecessor (or successor) is small, a pattern with a selected wavelength is established.[33] When overlap is significant, e.g., when $v > v_{c2}$ or $A = 0$, there is no wavelength selection[33] and the pattern is time dependent.[28]

2. When $t < \tau$, the groove amplitude $f_1 \sim \sqrt{t}$ suggesting its growth is like diffusion (Fig. 6b). While the diffusion equation predicts that a δ-function *decays* irreversibly via Gaussians, here, the Gaussian grooves *sharpen* like $\sqrt{t}$, implying a self-organizing process not classical diffusion. Furthermore, $\langle \xi_0 \rangle \sim 2\pi(l_T \hat{d})^{1/2}$: the displacement of the groove relative to the flat interface because of impurity increase at the groove is comparable to groove curvature [Eq. (1)]. Thus, except during the initial transient, curvature effects are not negligible during groove formation.

3. When $\tau > t > \tau/5$,

$$\frac{z_I(x,t) - z_0 - f_1(t)}{-f_1(t)} = f$$

with f independent of time, is an excellent approximation. When $t > \tau/5$, the Gaussians in Fig. 6a are nearly the same when f_1 is scaled out.

4. While a groove deepens relative to the flat interface, the tip advances, preparing the site of the next groove position in the propagating pattern (Fig. 2). The picture is that groove formation introduces a localized modulation in an initially uniform concentration profile parallel to the interface. To sustain its initial growth, the groove drains impurities from the tip region. Once groove curvature is sufficient to maintain its displacement for a given boundary condition, δ in Eq. (1), the next groove starts. The uniform rate of groove formation then emerges as a consequence of boundary conditions set by the solid–liquid interface.

5. A theory is needed to explain why the grooves should or should not be Gaussian. Here we only point out that Gaussians are a natural choice if one imposes localization on the groove shape, that is, requiring z_l and all its derivatives to be zero at $\pm\infty$ and $dz_l/dx = 0$ at $x = 0$ where z_l is maximum. It would also be interesting to know if wavelength selection results when a parabolic shape[13] is required for the tip and a Gaussian shape for grooves.

These measurements supplement information obtained on the cell shape in the tip region of the cellular pattern[38] and show how impurities, driven by curvature, self-organize in solidification. Furthermore, the system achieves this starting from a localized perturbation with zero initial curvature. As the amplitude grows, the half-widths decrease until the groove curvature balances its displacement from the planar interface. As far as we know, they are the first measurements of groove shapes at the solid–liquid interface. An impressive feature is that once grooves form parallel to the side walls, a stationary wavelength is established.

6. CONCLUSIONS

We have prepared a cellular pattern with a well-defined wavelength in directional solidification when $y_0 \sim \lambda = 100\ \mu$m. While there is not yet a theory to describe our observations, prepared patterns are expected to more closely resemble the ideal patterns of theory. We have shown that when the pattern evolves from front propagation in a ramp, it has a well-defined wavelength and is asymmetric: the grooves are parallel to the capillary side walls (boundary effect), whereas cell tips are perpendicular to $\mathbf{v}$ (the driving force). Boundary effects are essential in the preparation of this pattern. When $\varepsilon \gtrsim 0$, the groove shapes are two-dimensional and Gaussian, suggesting that, in contrast to a sinusoidal perturbation, the grooves in Fig. 6a are a response to a local perturbation. While a broad band of wavelengths are unstable for sinusoidal perturbations, wavelength selection may be a consequence of a local perturbation if $v < v_{c2}$. Close to threshold in the self-organization process, the groove amplitude grows like $\sqrt{t}$ and the half-widths decrease like $1/t^{1/4}$.

ACKNOWLEDGMENTS

It is a pleasure to acknowledge useful and stimulating discussions with H. R. Brand, J. T. Gleeson, Akira Hasegawa, and W. van Saarloos and to thank the conference organizers for their support.

REFERENCES

1. J. S. Langer, *Rev. Mod. Phys.* **52**:1 (1980); in *Chance and Matter*, J. Souletie, J. Vannimenus, and R. Stora, eds. (Elsevier, New York, 1986), p. 629; *Science* **243**:1150 (1989).
2. *Pierre Pelcé*, ed., *Dynamics of Curved Interfaces* (Academic Press, New York, 1988).
3. J. E. Wesfreid, H. R. Brand, P. Manneville, G. Albinet, and N. Boccara, eds., *Les Houches 1987, Propagation in Systems far from Equilibrium* (Springer-Verlag, 1988); F. Busse and L. Kramer, eds., *Non-linear Evolution of Spatio-Temporal Structures in Dissipative Continuous Systems* (Plenum Press, New York, 1990); D. Walgraef and N. Ghoniem (eds.), *Defects, Patterns and Instabilities* (Kluwer Academic Publishers, 1990); Lui Lam and Hedley C. Morris, eds., *Non-linear Structures in Physical Systems—Pattern Formation, Chaos and Waves* (Springer-Verlag, 1990).
4. P. Pfeuty and G. Toulouse, *Introduction to the Renormalization Group and to Critical Phenomena* (Wiley, New York, 1977).
5. P. C. Hohenberg and M. C. Cross, in *Fluctuations and Stochastic Phenomena in Condensed Matter*, L. Garrido, ed. (Springer-Verlag, Berlin, 1987).
6. W. Bascom, *Waves and Beaches, the Dynamics of the Ocean Surface* (Doubleday, New York, 1980).
7. J. D. Legrange, *Phys. Rev. Lett.* **66**:37(1991); J. E. Riegler and J. D. Legrange, *Phys. Rev. Lett.* **61**:2492 (1988).
8. S. M. Troian, E. Herbolzheimer, and S. A. Safran, *Phys. Rev. Lett.* **65**:333 (1990).
9. J. Bechhoefer and A. Libchaber, *Phys. Rev. B* **35**:1393 (1987); P. Oswald, J. Bechhoefer, and A. Libchaber, *Phys. Rev. Lett.* **58**:2318 (1987); A. J. Simon, J. Bechhoefer, and A. Libchaber, *Phys. Rev. Lett.* **61**:2574 (1988).
10. P. G. Saffman and G. I. Taylor, *Proc. R. Soc. Lond. A* **245**:312 (1958).
11. M. Rabaud, S. Michalland, and Y. Couder, *Phys. Rev. Lett.* **64**:184 (1990).
12. B. R. Pamplin, ed., *Crystal Growth* (Pergamon, Oxford, 1980).
13. Ph. Bouissou, A. Chiffaudel, B. Perrin, and P. Tabeling, *Europhysics Lett.* **13**:89 (1990); Phillippe Bouissou, thesis, Ecole Normale Supérieure, Paris (1989).
14. A. Dougherty, P. D. Kaplan, and J. P. Gollub, *Phys. Rev. Lett.* **58**:1652 (1987).
15. A. Schenzle and H. R. Brand, *Phys. Rev. A* **20**:1628 (1979).
16. R. J. Deissler and H. R. Brand, *Phys. Lett. A* **130**:293 (1988); R. J. Deissler, *J. Stat. Phys.* **54**:1459 (1989); *Physica D* **25**:233 (1987).
17. K. A. Jackson and J. D. Hunt, *Acta Met.* **13**:1212 (1965).
18. W. W. Mullins and R. F. Sekerka, *J. Appl. Phys.* **34**:323 (1963); **35**:444 (1964).
19. J. D. Hunt and K. A. Jackson, *Trans. Met. Soc. AIME* **236**:843, 1129 (1966).
20. K. A. Jackson, in *Material Science Research*, Vol. 4, Chapter 12 (Plenum Press, New York, 1969); *J. Crystal Growth* **24/25**:130 (1974).
21. H. Levine, in *Defects, Patterns and Instabilities*, D. Walgraef and N. Ghoniem (eds.). (Kluwer Academic Publishers, 1990).
22. J. D. Weeks and W. van Saarloos, *Phys. Rev. A* **42**:5056 (1990).
23. W. Kurz and D. J. Fisher, *Fundamentals of Solidification*, 3rd rev. ed. (Trans Tech Publications, Vermont, 1989).
24. A. Karma, *Phys. Rev. Lett.* **57**:858 (1986); T. Dombre and V. Hakim, *Phys. Rev. A* **36**:2811 (1987); M. Ben-Amar and P. Moussallam, *Phys. Rev. Lett.* **60**:317 (1988); C. Misbah, *J. Phys. (Paris)* **50**:971 (1989); K. Tsiveriotis and R. A. Brown, *Phys. Rev. Lett.* **63**:2048 (1989).
25. D. J. Wollkind and L. A. Segel, *Phil. Trans. R. Soc. Lond.* **51**:268 (1970).
26. J. S. Langer and L. A. Turski, *Acta Met.* **24**:1113 (1977); J. S. Langer, *Acta Met.* **25**:1121 (1977); G. Dee and R. Mathur, *Phys. Rev.* **27**:7073 (1983).

27. M. A. Eshelman and R. Trivedi, *Acta Met.* **35**:2443 (1987).
28. P. E. Cladis, J. T. Gleeson, and P. L. Finn, in *Defects, Patterns and Instabilities*, D. Walgraef and N. Ghoniem (eds.). (Kluwer Academic Publishers, 1990).
29. G. Dee and J. S. Langer, *Phys. Rev. Lett.* **50**:383 (1983).
30. P. E. Cladis, J. T. Gleeson, and P. L. Finn, *Phys. Rev. Lett.*, submitted.
31. L. Kramer, E. Ben-Jacob, H. R. Brand, and M. C. Cross, *Phys. Rev. Lett.* **49**:1891 (1982); see also L. Kramer and P. C. Hohenberg, *Cellular Structures in Instabilities*, J. E. Wesfreid and S. Zaleski, eds. (Springer-Verlag); L. Kramer and H. Riecke, *Z. Phys. B* **50**:245 (1985).
32. P. Coullet, R. E. Goldstein, and G. H. Gunaratne, *Phys. Rev. Lett.* **63**:1954 (1989); R. E. Goldstein, G. H. Gunaratne, L. Gil, and P. Coullet, Hydrodynamic and interfacial patterns with broken space-time symmetry (preprint 5/1990).
33. P. E. Cladis, J. T. Gleeson, and P. L. Finn, in *Non-linear Evolution of Spatio-Temporal Structures in Dissipative Continuous Systems*, F. Busse and L. Kramer, eds. (Plenum Press, New York, 1990); also in *Non-linear Structures in Physical Systems—Pattern Formation, Chaos and Waves*, Lui Lam and Hedley C. Morris, eds. (Springer-Verlag, 1990).
34. M. A. Chopra, M. E. Glicksman, and N. B. Singh, *J. Cryst. Growth* **543**:543 (1988).
35. B. Caroli, C. Caroli, and B. Roulet, *J. Phys. (Paris)* **43**:1767 (1982).
36. J. T. Gleeson *et al.*, unpublished.
37. W. van Saarloos, *Phys. Rev. A* **39**:6367 (1990) and references therein.
38. P. Kurowski, C. Guthmann, and S. de Cheveigné, *Phys. Rev. A* **42**:7368 (1990); P. Kurowski, Thesis, University of Paris VII (1990).
39. J. T. Gleeson, P. L. Finn, and P. E. Cladis, *Phys. Rev. Lett.* **66**:236 (1991).
40. J. D. Weeks and W. van Saarloos, *Phys. Rev. A* **39**:2772 (1989); J. D. Hunt, *Solidification and Casting of Metals* (Metals Society, London, 1979).
41. S. de Cheveigné, C. Guthmann, and M. M. Lebrun, *J. Phys. (Paris)* **47**:2095 (1986).